Applied Mathematical Modelling 42 (2017) 576–590

Contents lists available at ScienceDirect

Applied Mathematical Modelling

journal homepage: www.elsevier.com/locate/apm

Modeling the impact of discretizing rotor angular position on computation of field-oriented current components in high speed electric drives

Leszek Jarzebowicz

Faculty of Electrical and Control Engineering, Gdansk University of Technology, Narutowicza St. 11/12, 80-233 Gdansk, Poland

ARTICLE INFO

Article history:
Received 25 February 2016
Revised 29 September 2016
Accepted 19 October 2016
Available online 24 October 2016

Keywords:
Alternating current (AC) electric drives
Current sampling
Digital control
Field-oriented control
Hybrid discrete-continuous modeling

ABSTRACT

Modern drives consist of alternating current electric motors, and the field-oriented control (FOC) of such motors enables fast, precise, and robust regulation of a drive's mechanical variables such as torque, speed, and position. The control algorithm, implemented in a microprocessor, requires feedback from motor currents, and the quality of this feedback is essential to a drive's control properties. Motor phase currents are sampled and processed in order to extract their mean over a digital control interval. Afterwards, the mean phase currents are transformed into a rotating field-oriented reference frame to enable controlling the mechanical variables. The field-oriented frame rotates continuously, but in practice the transformation is carried out using a discrete angular position. This paper investigates how the discretization impacts the computed field-oriented currents in high speed drives, where the rotor displacement during a control interval is substantial. A continuous-time model of field-oriented currents is indicated as a reference to quantify errors. An original approach to normalize variables and to solve the model analytically is proposed in order to investigate how the errors related to rotor position discretization are influenced by drive operating conditions. The analytical solution is validated by computer simulation. The results show that the currently applied methodology of computing field-oriented current components, due to an invalid assumption, introduces errors of a few percent when a drive operates at high speed. These errors can be compensated using the presented solution.

1. Introduction

Digitally controlled electric drives are present in numerous devices and systems, and they have to face increasing demands regarding control precision, efficiency, and robustness [1]. There are applications such as electric vehicles or home appliances that combine the above-listed general demands with a requirement of extended speed range operation [2]. Due to the progress in control methods and motor designs, drive operational speed range has extended, for example the maximal speed of an electric drive applied to the latest Toyota Prius reaches 13,500 rpm [3], which is more than double compared with the first generation of Prius introduced in 1997.

Modern drives consist of alternating current (AC) electric machines like induction motors (IM) or permanent magnet synchronous motors (PMSM), with such motors enabling fast, precise, and robust control of mechanical variables. The

E-mail address: leszek.jarzebowicz@pg.gda.pl

http://dx.doi.org/10.1016/j.apm.2016.10.046
0307-904X/

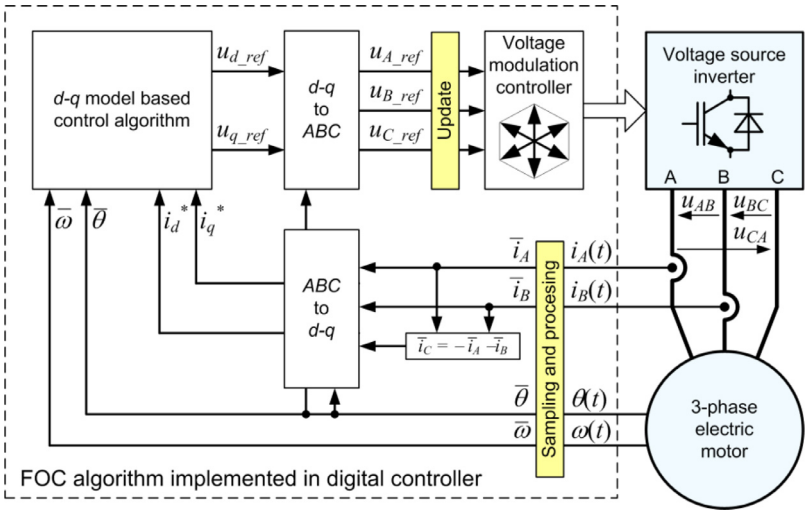

Fig. 1. General structure of FOC applied to PMSM drive.

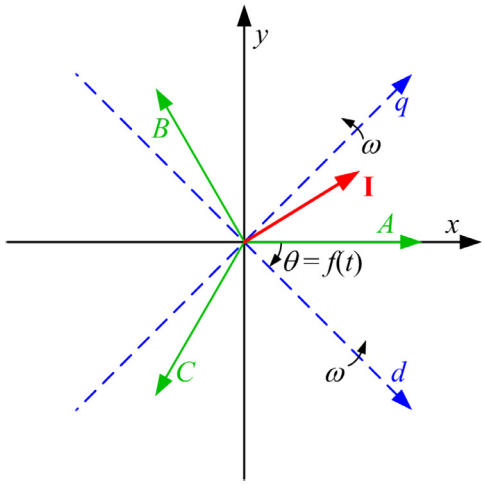

Fig. 2. Reference frames used for modeling and control of PMSM drives.

fundamental control concerns torque, which is related to motor currents in three-phase windings fixed to the stator. As the currents can be regulated rapidly and precisely, the same applies to the torque. Rotor speed and position are controlled by shaping a motor's torque in time, and thus the control of all the mechanical variables is strictly related to regulating motor currents.

Controlling currents require the means to apply variable voltages to the motor terminals and to measure the actual motor currents. Hence, the drives consist of a voltage source inverter and currents' feedback (Fig. 1). The inverter supplies the motor with voltages that have values set by the control algorithm for subsequent discrete control intervals. The currents' feedback enables the algorithm to control the voltages in the closed-loop manner. Typically, two out of three currents i_A, i_B, i_C are physically measured. The third one is computed assuming that the sum of the currents is zero.

Under steady operating conditions, the motor phase currents i_A, i_B, i_C are quasi-sine wave shaped, but during control transients their waveforms are complex and cannot be parameterized by amplitude and frequency. Thus, the drives dedicated to dynamic control use vector control approach [4], which represents motor phase currents by a vector with a modulus and angle that can change rapidly to follow transients. This current vector can be expressed as $\mathbf{I}(i_A, i_B, i_C)$ by using *ABC* coordinates that correspond to the physical layout of motor windings *A*, *B*, and *C*. In order to reduce the number of variables required to define the vector, an *x*–*y* reference frame, as shown in Fig. 2, is commonly used to describe motor currents with two scalar variables i_x and i_y.

In stationary reference frames *ABC* and *x*–*y*, the relation between the motor's torque and currents is complex and involves a rotor position that advances while the rotor revolves. Hence, for control purposes, it is convenient to use a rotating reference frame marked *d*-*q*, with a *d*-axis fixed to the rotor's magnetic field. Such an approach is called field-oriented con-

trol (FOC) [5]. As the torque is described by a straightforward dependency from *d*- and *q*- components of the current vector, the control structure formulated for *d-q* motor model is simple. The structure of FOC for PMSM is shown in Fig. 1.

Contemporary electric drives are digitally controlled, thus a control algorithm's output is updated in discrete time instants spaced by control interval *T*. As motor circuits consist of inductances that accumulate energy, it is inevitable that motor currents change during control intervals, even under constant supplying voltages. The digital control algorithm aims at regulating currents in terms of their mean values $\bar{i}$ (the dash indicates mean here and later in the text) determined individually for each discrete control interval. Thus, to provide a control algorithm with suitable feedback, specific methods of sampling and processing currents are used, with outcomes $\bar{i}$ that aim to satisfy the formula:

$$\bar{i} = \frac{1}{T}\int_0^T i(t)dt. \tag{1}$$

While these sampling and processing methods deliver mean phase currents $\bar{i}_A$, $\bar{i}_B$, $\bar{i}_C$, the control algorithm requires $\bar{i}_d$, $\bar{i}_q$ feedback since it regulates torque based on the field-oriented components of the current vector. Thus, for every control period, the mean phase currents are transformed from co-ordinates of the stationary *ABC* frame into the flux-oriented *d-q* frame, which rotates synchronously with the rotor [6], as shown in Fig. 2. This is done using Clarke transform first:

$$\begin{bmatrix}\bar{i}_x\\ \bar{i}_y\end{bmatrix} = \frac{2}{3}\begin{bmatrix}1 & -1/2 & -1/2\\ 0 & \sqrt{3}/2 & -\sqrt{3}/2\end{bmatrix}\begin{bmatrix}\bar{i}_A\\ \bar{i}_B\\ \bar{i}_C\end{bmatrix}, \tag{2}$$

and then Park transform:

$$\begin{bmatrix}i_d{}^*\\ i_q{}^*\end{bmatrix} = \begin{bmatrix}\cos\bar{\theta} & \sin\bar{\theta}\\ -\sin\bar{\theta} & \cos\bar{\theta}\end{bmatrix}\begin{bmatrix}\bar{i}_x\\ \bar{i}_y\end{bmatrix}, \tag{3}$$

where: $\bar{\theta}$ is the discretized (mean) rotor position.

These transforms were originally derived for converting instantaneous vectors. In digitally controlled drives, they are used to recalculate values that represent the mean over a period *T*, and thus the impact of discretization on the outcomes shall be investigated. The Clarke transform matrix consists of constants, and hence its application to discretized currents introduces no constraints. Nevertheless, the Park transform (3) uses the discrete angle $\bar{\theta}$, while in fact the angle $\theta(t)$ is a continuous function of time, and the range of its changes within the control interval increases with rotor speed. Providing the Park transform with mean phase currents $\bar{i}_A$, $\bar{i}_B$, $\bar{i}_C$ and discretized rotor position $\bar{\theta}$ causes outcomes $i_d{}^*$ and $i_q{}^*$ to represent the components $\bar{i}_d$, $\bar{i}_q$ of the mean field-oriented current vector only in an approximate manner. Therefore, the trend of extending operational speed range raises the question of whether the existing approach of determining mean *d-q* current components is still appropriate for modern high-speed drives. This study investigates the errors of the present approach to computing mean flux-oriented currents, by comparing the results of discrete-angle computation (3) with the outcomes of a reference continuous-time model as described in Section 3. The contribution of the present work consists of:

- indicating the problem of discretizing the rotor position in high speed electric drives;
- formulating a continuous-angle processing approach as a reference for error computation;
- proposing a methodology to parameterize and solve the continuous-angle formula analytically;
- quantifying the errors in field-oriented current components related to discretizing rotor position;
- developing a test-scenario for validating the analytical solution by computer simulation.

2. State of the art

The methodology of current sampling and processing in digitally-controlled electric drives has well settled since microcontrollers were introduced into these applications [7]. However, recent research has revealed some limitations and introduced new solutions to current measurements and processing. *Kim* et al. [8] analyzed measurement errors introduced by the imperfections of current feedback hardware. The impact of scaling and offset errors in particular motor phase current sensors on a drive performance was analyzed and a suitable error compensation method was proposed. *Wolf* et al. indicated that there are cases where motor phase currents should not be approximated with linear functions [9], particularly in modeling motors with relatively small electrical time constants and long control cycle durations. The authors analyzed how the assumption of linear current changes affects the accuracy of the mean phase currents measurement. In turn, *Bocker* and *Buchholz* investigated the impact of the currents' sampling rate on drive control dynamics [10], proving that current oversampling with a ratio of 8–16 combined with applying a specific PWM generator, which allows for multiple reference updates within the control intervals, significantly improves the control properties of an electric drive. There are also attempts to predict future current values based on the electric drive model and to use the predicted values for improvement of control dynamics, for example the attempt presented by *Wang* et al. [11]. An interesting predictive approach including compensation of computation delay was proposed by *Cortes* et al. [12].

Control algorithms for AC drives are constantly being improved. This also applies to solutions dedicated for operating at an extended speed range, i.e. in the so-called flux weakening region. In order to increase a drive's torque at high speeds,

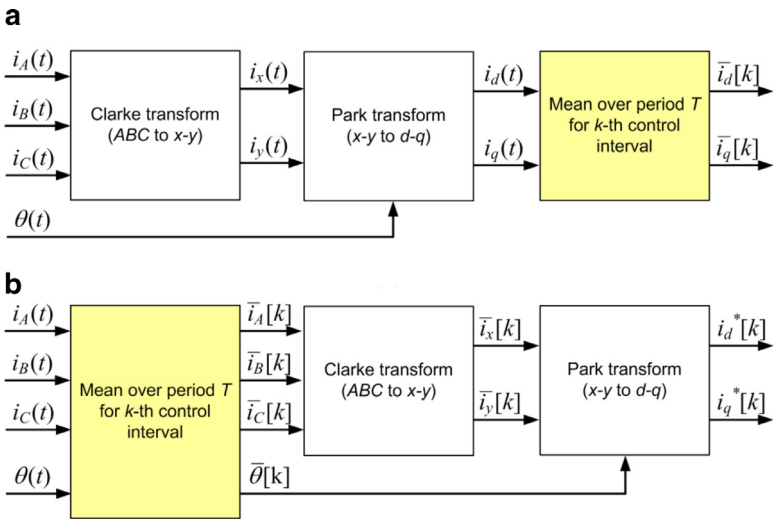

Fig. 3. Algorithms for computing flux-oriented current vector components in the k^{th} control cycle: (a) mathematically correct approach; (b) practically applied approach.

it is commonly proposed to use a six-step control mode that fully utilizes the supply voltage [13,14]. In such a mode, motor supply voltages are updated only six times per rotor revolution. Until recently, a simplified control approach was applied for the six-step operation, which is based on predefined look-up tables, where input variables consist of required torque and measured speed. *Kwon* et al. [15] proposed a new control approach for PMSM which sustains the field-oriented current components regulation. Their control algorithm has superior dynamic properties that are important, for example, for vehicles' traction control systems such as ABS or ESP applied in electric and hybrid cars [16].

Mathematical models of electric motors have also been improved in order to increase control robustness and precision. *Racewicz* et al. investigated the influence of motor core saturation on model topology and parameters [17], suggesting that motor inductances should be formulated as half-order functions as this will lead to better convergence of the model. In turn, *Tudorache* and *Trifu* proposed using a hybrid numerical-analytical model to optimize the design of PMSM in terms of cogging torque [18]. *Rodriguez* et al. introduced a multi-physical PMSM model that couples electrical, magnetic, thermal, and vibro-acoustic phenomena, and which may be used for very accurate simulation of motor behavior. *Vittek* et al. [19] expanded the mechanical subsystem in the PMSM model in order to cover elastic properties of motor shaft coupling. When applied to a state observer, the subsystem significantly improves the precision of controlling load-side shaft position.

3. Problem formulation

As indicated in the previous section, recently introduced control methods require precise $\bar{i}_d$ and $\bar{i}_q$ currents feedback for high performance torque control at medium and high speeds, when the six-step control mode is applied. While research on current measurements focuses either on accuracy of determining the motor mean phase currents $\bar{i}_A$, $\bar{i}_B$, $\bar{i}_C$ or on predicting current values in forthcoming control cycles, no attention is paid to the impact of rotor position discretization on computing mean *d*- and *q*- current components.

The mechanical time constant of the motor is very large when compared with the electrical one, and thus it may be concluded that the rotor speed is constant when considering electric transients. Nevertheless, the assumption that changes in rotor position during the control interval T are negligible does not hold in the six-step mode where the rotor may revolve by as much as $\pi/3$ rad. New models of electric drives, although increasingly detailed and accurate, do not emphasize the impact of discretization in the transformation of the variables, which is important for digital implementation of contemporary control algorithms.

As the rotor revolves continuously, the same applies to the field-oriented reference frame. Hence, the precise field-oriented mean currents shall be derived by applying the Park transform to continuous motor currents first and then by computing their mean. Such an approach is depicted in Fig. 3a and described by the following formula:

$$\begin{cases} \bar{i}_d = \dfrac{1}{T}\displaystyle\int_0^T i_d(t)dt = \dfrac{1}{T}\int_0^T \cos(\theta(t))\cdot i_x(t)dt + \dfrac{1}{T}\int_0^T \sin(\theta(t))\cdot i_y(t)dt \\ \bar{i}_q = \dfrac{1}{T}\displaystyle\int_0^T i_q(t)dt = \dfrac{1}{T}\int_0^T -\sin(\theta(t))\cdot i_x(t)dt + \dfrac{1}{T}\int_0^T \cos(\theta(t))\cdot i_y(t)dt \end{cases} \quad (4)$$

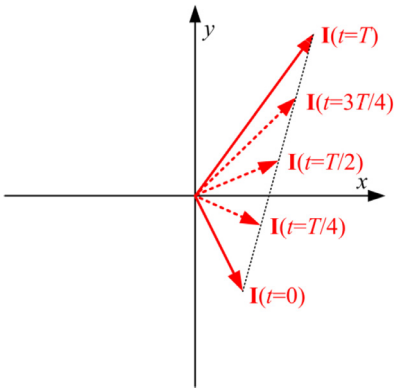

Fig. 4. A track of current vector changes on the stationary reference plane *x–y*.

The contemporary practice of deriving mean phase currents and then transforming them into the field-oriented frame, as shown in Fig. 3b and described by (3), matches the precise processing approach (4) only with the assumption that $\theta(t) = \overline{\theta} = const.$, which is not appropriate for the six-step mode. The aim of this study is to investigate the impact of discretizing rotor angular position on the determined mean flux-oriented current components during the six-step drive operation. The error, defined as a difference between results of continuous-time processing (4) and discrete-angle approach (3), is derived analytically and its correlation with drive operating conditions is researched.

This research was initiated in [20], where a simplified model for the estimation of steady-state error analysis was proposed. In this paper the errors are computed using (4) without oversimplifications, both for steady condition and transients.

4. Analytical analysis of discrete-angle processing errors

4.1. Basic assumptions on motor current behavior

A current vector in a stationary reference plane (superscript (s)) can be described by scalars referring to either *ABC* or *x–y* co-ordinates as follows:

$$\mathbf{I}^{(s)}(t) = i_A(t) + i_B(t)\exp\left(\mathbf{j}\frac{2}{3}\pi\right) + i_C(t)\exp\left(\mathbf{j}\frac{4}{3}\pi\right) = i_x(t) + \mathbf{j}i_y(t). \tag{5}$$

The reference frames *ABC* and *x–y* are both stationary and transforming the vector between these two frames is not affected by rotor movement. For convenience, only the *x–y* frame is used later on to describe stationary motor currents.

The analysis focuses on motor currents' behavior during a single control interval, i.e. in a time range from $t = 0$ to $t=T$. In the six-step control mode, motor supply voltages are steady during a control interval, and thus motor phase currents are approximated by linear functions [21]. *Wolf* et al. indicated that this approximation in some cases leads to non-negligible errors [9], and so numerical computations were performed afterwards, and presented in Section 5, in order to validate the linear currents assumption.

According to the assumption of linear phase currents, the current vector observed in the stationary plane *x–y* traces a straight line with a constant speed, as shown in Fig. 4. Moreover, the instantaneous value of $\mathbf{I}^{(s)}$ at $t=T/2$ corresponds with the mean over a period *T*. So the vector representing mean currents in a stationary reference frame is equal to the instantaneous current vector in the middle of the control interval, i.e. $\overline{\mathbf{I}}^{(s)} = \mathbf{I}^{(s)}(t = T/2)$.

The instantaneous current vector observed in the rotating reference frame (superscript (r)) is expressed as:

$$\mathbf{I}^{(r)}(t) = i_d(t) + \mathbf{j}i_q(t) = \mathbf{I}^{(s)}(t)\exp\left(-\mathbf{j}\theta(t)\right), \tag{6}$$

where the rotor position is given by $\theta(t) = \omega t$, since rotor speed ω can be assumed constant due to a relatively high mechanical moment of inertia.

The vector $\mathbf{I}^{(r)}(t)$ changes in a non-linear manner due to the exponential part of (6). As a result, the vector representing the mean currents in the rotating reference frame is not equal to the instantaneous current vector in the middle of the control interval. Thus, the relation (6) formulated for instantaneous vectors is not valid for the variables representing mean

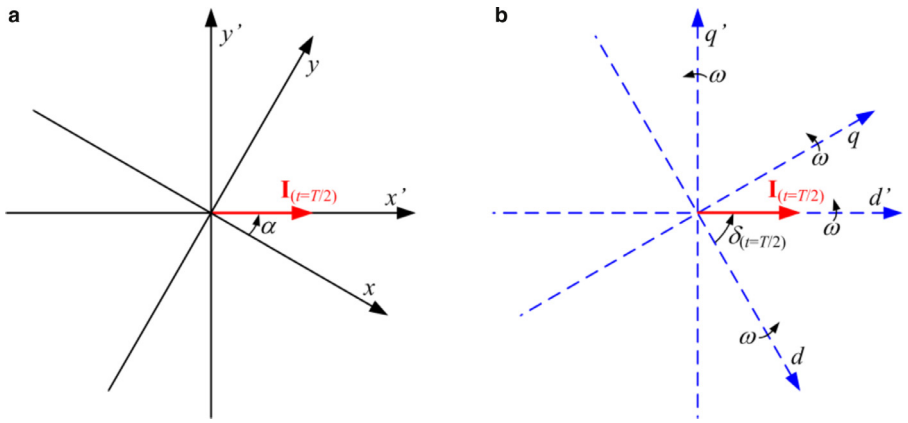

Fig. 5. MPCA reference frames: x'–y' (a) and d'–q' (b).

values, i.e. $\bar{\mathbf{I}}^{(r)} \neq \bar{\mathbf{I}}^{(s)} \exp(-\mathbf{j}\bar{\theta}(t))$. Differences in angle and modulus between vector quantities at both sides of this equation correspond to errors of discrete-angle current processing.

4.2. Normalization of co-ordinates

The differences between outcomes of continuous-angle (4) and discrete-angle (3) processing depend on the input functions $i_x(t)$, $i_y(t)$, and $\theta(t)$. These functions are random in subsequent control intervals, even under steady drive operation. Thus, an original methodology is proposed to reformulate the input functions so that they relate to the field-oriented current vector. This way the input functions describe the drive's operating conditions, so their impact on discrete-angle (3) processing can be investigated. Moreover, the methodology leads to simple formulae, which can be solved analytically without any approximation.

The methodology consists of two-way normalization:

(1) Modulus normalization introduces a per-unit system for current vector length. The base unit corresponds to the modulus of the current vector at the instant of $t=T/2$, so it also corresponds to the modulus of the mean current vector computed in stationary reference frame x–y, i.e. $I_{base} = |\mathbf{I}(t = T/2)| = |\bar{\mathbf{I}}^{(s)}| = 1$ p.u.

(2) Angle normalization introduces two additional reference frames, x'-y' and d'-q', called mean-phase-current-aligned (MPCA) frames. The x'-y' frame is stationary and angularly shifted with respect to the original x–y frame by an angle α = const., as shown in Fig. 5. The d'-q' frame rotates synchronously to the original d-q frame, and is angularly shifted with respect to d-q by an angle δ = const. The angles α and δ are selected so that at the instant $t=T/2$, the axes x' and d' are aligned to the current vector $\mathbf{I}$. Thus, the angular displacement between the aligned reference frames d'-q' and x'-y' equals $\theta'(t)=\theta(t)+\alpha-\delta$.

Transformation between the original reference frames and the MPCA frames involves constant angles α and δ, and therefore it is not affected by changes in rotor angular position $\theta(t)$. Consequently, in every particular case the difference between mean current vectors computed using continuous-angle and discrete-angle approaches is the same whether the input functions are formulated in the original or in the MPCA frames. However, using the normalization is convenient because:

- it is easy to formulate $i_{x'}(t)$ and $i_{y'}(t)$ functions whose parameters correspond to drive operating conditions, as discussed in the following subsection;
- $\theta'(t)$ is a linear and odd function, which assures that integration intervals over $\theta'(t)$ are symmetrical; this, in turn, makes it possible to solve the model equations formulated in Section 4.4 analytically by substituting time t as a function of the angle θ';
- the result of the discrete-angle processing equals $\mathbf{I}_{d'-q'}(t=T/2)=1+\mathbf{j}0$, so it is easy to derive the error by comparing the outcome of continuous-angle processing with a unit vector, as described in Section 4.5.

4.3. Formulation of input functions

Formulation of functions $i_{x'}(t)$, $i_{y'}(t)$, and $\theta(t)$ is derived first for the steady operating condition, after which the general case that allows for modeling transients is described. A steady state in the FOC algorithm is defined as a case when motor currents observed in the d-q rotating reference frame at instants $t = 0$ and $t=T$ are equal. The same applies to d'-q' oriented currents, i.e. $\mathbf{I}_{d'-q'}(t = 0)=\mathbf{I}_{d'-q'}(t = T)$. Moreover, in steady state the reference angle of the voltage vector in the rotating

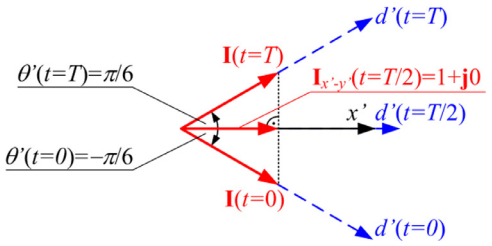

Fig. 6. Modeling the input functions for MPCA frames in steady control state (presented on a stationary plane).

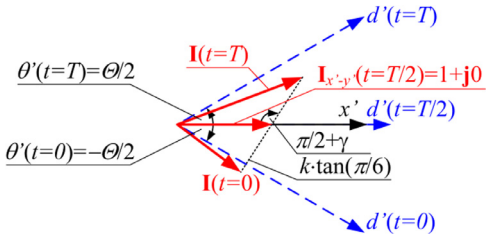

Fig. 7. Modeling the input functions for MPCA frames during a control transient (presented on a stationary plane).

co-ordinate frame is constant, and thus the rotor position changes during the control interval by an angle of $\pi/3$ rad. Such a case is depicted in Fig. 6 and described by the following set of input functions:

$$\begin{cases} i_{x'}(t) = 1 = const. \\ i_{y'}(t) = \tan(\pi/6) \cdot (2t/T - 1) \\ \theta'(t) = \pi/6 \cdot (2t/T - 1) \end{cases}. \tag{7}$$

During a transient, the value of $\mathbf{I}_{d'\text{-}q'}(t = T)$ differs with respect to $\mathbf{I}_{d'\text{-}q'}(t = 0)$. Moreover, the duration of control interval T may vary, and thus the angular distance Θ covered by the rotor may differ from $\pi/3$ rad. The changes in control interval duration are expected to be smooth in usual operating conditions, but they should still be reflected in the model to minimize the number of simplifications. The behavior of the current vector in MPCA reference frames for a case of transients is depicted in Fig. 7. The changes in current vectors are parameterized by variables k and γ, which are not directly related to parameters used in a control algorithm, but are selected to obtain simple input functions that can be later used to analytically derive errors of discrete-angle processing.

The set of input functions corresponding to the general case, including transients, is given by (8). Steady state operation may be considered a particular case when $k = 1$, $\gamma = 0$, and $\Theta = \pi/3$ rad.

$$\begin{cases} i_{x'}(t) = 1 + k \cdot \sin\gamma \cdot \tan(\pi/6) \cdot (2t/T - 1) \\ i_{y'}(t) = k \cdot \cos\gamma \cdot \tan(\pi/6) \cdot (2t/T - 1) \\ \theta'(t) = \Theta/2 \cdot (2t/T - 1) \end{cases}. \tag{8}$$

4.4. Analytical solution of continuous-angle formula

Applying the input functions (7) and (8) into the continuous-angle formula (4) allows for computing accurate MPCA components $\bar{i}_{d'}$ and $\bar{i}_{q'}$ of the mean current vector in the field-oriented reference frame. Due to the normalization, the mean current vector computed using discrete-angle formula is a unit vector, and so any deviations of $\bar{i}_{d'}$ and $\bar{i}_{q'}$ from 1 and 0, respectively, indicate errors in the discrete-angle processing approach. For operating at steady state, the MPCA components $\bar{i}_{d'}$ and $\bar{i}_{q'}$ are given by:

$$\begin{cases} \bar{i}_{d'(steady)} = \dfrac{1}{T}\displaystyle\int_0^T \cos(\pi/6 \cdot (2t/T - 1)) \cdot 1dt + \dfrac{1}{T}\int_0^T \sin(\pi/6 \cdot (2t/T - 1)) \cdot (\tan(\pi/6) \cdot (2t/T - 1))dt \\ \qquad\qquad = 6\sqrt{3}/\pi^2 \cong 1.053 \\ \bar{i}_{q'(steady)} = \dfrac{1}{T}\displaystyle\int_0^T -\sin(\pi/6 \cdot (2t/T - 1)) \cdot 1dt + \dfrac{1}{T}\int_0^T \cos(\pi/6 \cdot (2t/T - 1)) \cdot (\tan(\pi/6) \cdot (2t/T - 1))dt = 0 \end{cases}. \tag{9}$$

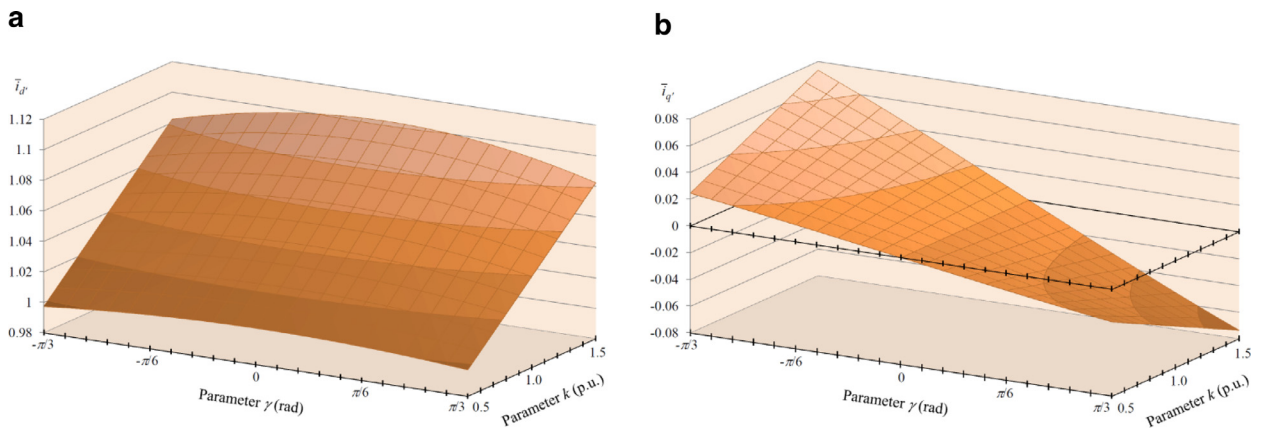

Fig. 8. Results of analytical computation of (4) using the normalized co-ordinates: d'-axis current component (a) and q'-axis current component (b).

The general solution of (4), with k, γ, and Θ used to parameterize transients, is given by (10). The impact of k and γ on the components $\bar{i}_{d'}$ and $\bar{i}_{q'}$ of the mean current vector is presented graphically in Fig. 8.

$$\begin{cases} \bar{i}_{d'(general)} = \dfrac{1}{T}\displaystyle\int_0^T \cos\left((\Theta/2)\cdot(2t/T-1)\right)\cdot\left(1+k\cdot\sin\gamma\cdot\tan(\pi/6)\cdot(2t/T-1)\right)dt+ \\ \qquad +\dfrac{1}{T}\displaystyle\int_0^T \sin\left((\Theta/2)\cdot(2t/T-1)\right)\cdot\left(k\cdot\cos\gamma\cdot\tan(\pi/6)\cdot(2t/T-1)\right)dt = \\ \qquad = (2/\Theta)\cdot\sin(\Theta/2)+k\cdot\cos\gamma\cdot\tan(\pi/6)\cdot\left(2/\Theta^2\right)\left(2\sin(\Theta/2)-\Theta\cos(\Theta/2)\right) \\ \bar{i}_{q'(general)} = \dfrac{1}{T}\displaystyle\int_0^T -\sin\left((\Theta/2)\cdot(2t/T-1)\right)\cdot\left(1+k\cdot\sin\gamma\cdot\tan(\pi/6)\cdot(2t/T-1)\right)dt+ \\ \qquad +\dfrac{1}{T}\displaystyle\int_0^T \cos\left((\Theta/2)\cdot(2t/T-1)\right)\cdot\left(k\cdot\cos\gamma\cdot\tan(\pi/6)\cdot(2t/T-1)\right)dt = \\ \qquad = -k\cdot\sin\gamma\cdot\tan(\pi/6)\cdot\left(2/\Theta^2\right)\cdot\left(2\sin(\Theta/2)-\Theta\cos(\Theta/2)\right) \end{cases} \tag{10}$$

The assumption of the linear motor phase currents leads to linear input functions $i_x'(t)$, $i_y'(t)$, and $\theta'(t)$. This, in turn, allows for the transformation of (9) and (10) into the sums of basic trigonometric integrals, and consequently to obtain the solution without using any advanced numerical or analytical methods. However, if the motor phase currents' non-linearity is approached, the input functions would consist of an additional exponential part parameterized with stator winding resistance and inductance of a particular motor. In such a case, solving (4) would require the use of sophisticated analytical methods such as the variational iteration method [22] or homotopy type approach [23].

4.5. Error computation

MPCA current components $\bar{i}_{d'}$ and $\bar{i}_{q'}$ computed in the previous subsection differ from 1 and 0, respectively, so they reveal discrepancies between continuous-angle and discrete-angle approaches. However, the MPCA co-ordinates, introduced in this paper, do not have a practical meaning for motor control purposes. To make the solution more informative, the results are converted to describe the errors in vector notation. Gain error is defined as the difference between the moduli of the mean current vectors obtained by continuous-angle and discrete-angle processing, and is computed as:

$$\delta|\mathbf{I}| = \sqrt{\left(\bar{i}_{d'}\right)^2+\left(\bar{i}_{q'}\right)^2}-1. \tag{11}$$

Phase error describes an angular difference between the mean current vectors computed using continuous-angle and discrete-angle formulae and is given by:

$$\delta\theta = \arctan\left(\bar{i}_{q'}/\bar{i}_{d'}\right). \tag{12}$$

Moreover, to co-relate the errors to drive operating conditions, these conditions are described by changes in the current vector modulus and angle occurring during a control interval, observed in the rotating reference frame. The change in the modulus is defined as:

$$\Delta\left|\mathbf{I}^{(r)}\right| = \left|\mathbf{I}^{(r)}(t=T)\right| - \left|\mathbf{I}^{(r)}(t=0)\right|, \tag{13}$$

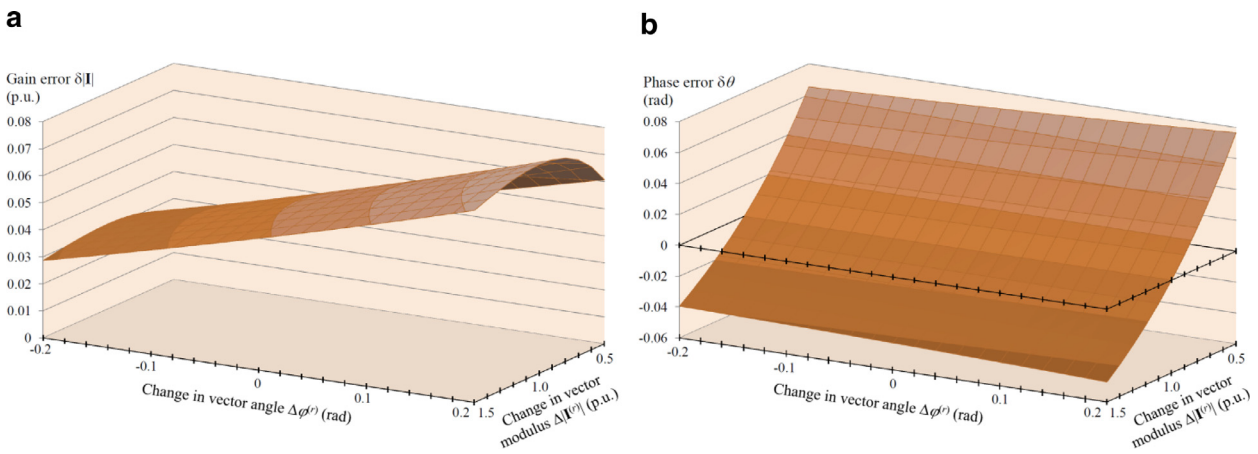

Fig. 9. Errors of discrete-angle computation of field-oriented mean current vector: gain error (a) and phase error (b).

and the change in the angle is given by:

$$\Delta\phi^{(r)} = \arg\left(\mathbf{I}^{(r)}(t=T)\right) - \arg\left(\mathbf{I}^{(r)}(t=0)\right). \tag{14}$$

The above definitions make it possible to present gain and phase errors of discrete-angle mean current vector computation as functions of changes in current vector modulus and angle, as depicted in Fig. 9. In steady state, represented by $\Delta|\mathbf{I}^{(r)}| = 0$ and $\Delta\varphi^{(r)} = 0$, the phase error is zero and the gain error is 5.3%. Such a gain error leads to substantial systematic deviation in the controlled currents. As the control algorithm is provided with an undervalued feedback, it unintentionally forces increased motor current. In transients, the gain error deviates from the value of 5.3%. The change in current vector modulus, both its increase and decrease, slightly decreases the gain error. The positive change in vector angle increases the error, contrary to the negative change. Also, during transients a phase error appears, and the value of this error is evidently much more sensitive to the change in vector modulus than angle.

The maximal changes in current vector modulus and angle depend on motor parameters, controller settings, and external operating conditions, so they are application specific. Therefore, it is not possible to evaluate peak errors of discretizing rotor angular position on the computation of the field-oriented current vector in general. Nevertheless, considering the average applications, the gain error is expected to reach 6–8% and the peak phase error may be at a level of 50 mrad.

5. Validation

5.1. Simulation model overview

Verification, based on computer simulation, is designed to validate the analytical derivation of errors in computing field-oriented currents related to the discrete-angle formula. The validation covers all the steps described in Section 4, but special attention is paid to the assumption of linear current changes. Details on approaching this assumption are given in Section 5.2.

The electric motor is represented by a three-phase symmetric *RL*-load, similar to the research on non-linearity of motor currents reported in [9]. Each motor phase is modeled by the following dependency:

$$u = R \cdot i + L\frac{di}{dt}, \tag{15}$$

where: u – motor phase voltage, i – motor phase current, R – motor stator resistance, and L – motor stator inductance. The equation incorporates the current non-linear behavior that is apparent when the ratio of the electrical time constant $\tau = R/L$ to the control interval duration T is below ten.

A typical six-transistor inverter is assumed to feed the motor. The inverter transistors are modeled to have ideal static and dynamic properties. An electrical diagram of the electric power system model of the drive is presented in Fig. 10.

The drive model also consists of a controller, which selects the inverter state with respect to the reference angle of voltage vector. The reference angle is defined in the rotating *d-q* co-ordinate frame, so upon stable reference the voltage vector observed in the stationary plane *x–y* rotates synchronously with the rotor. Only six active voltage vectors may be applied by the inverter: $(2/3)u_{DC}e^{\mathbf{j}(k-1)\cdot(\pi/6)}$, where $k = 1...6$. Thus, the active vector is selected as the one closest to the continuously rotating reference vector. The inverter model also produces a pulse-like signal that indicates the change in inverter state. The signal is used to mark control interval boundaries for mean-computing subsystems and for determining variables k, γ, and Θ from continuous motor current components.

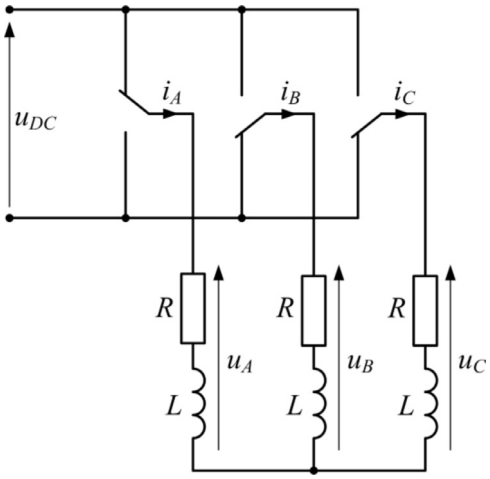

Fig. 10. Electrical diagram of a model representing an inverter-supplied electric motor.

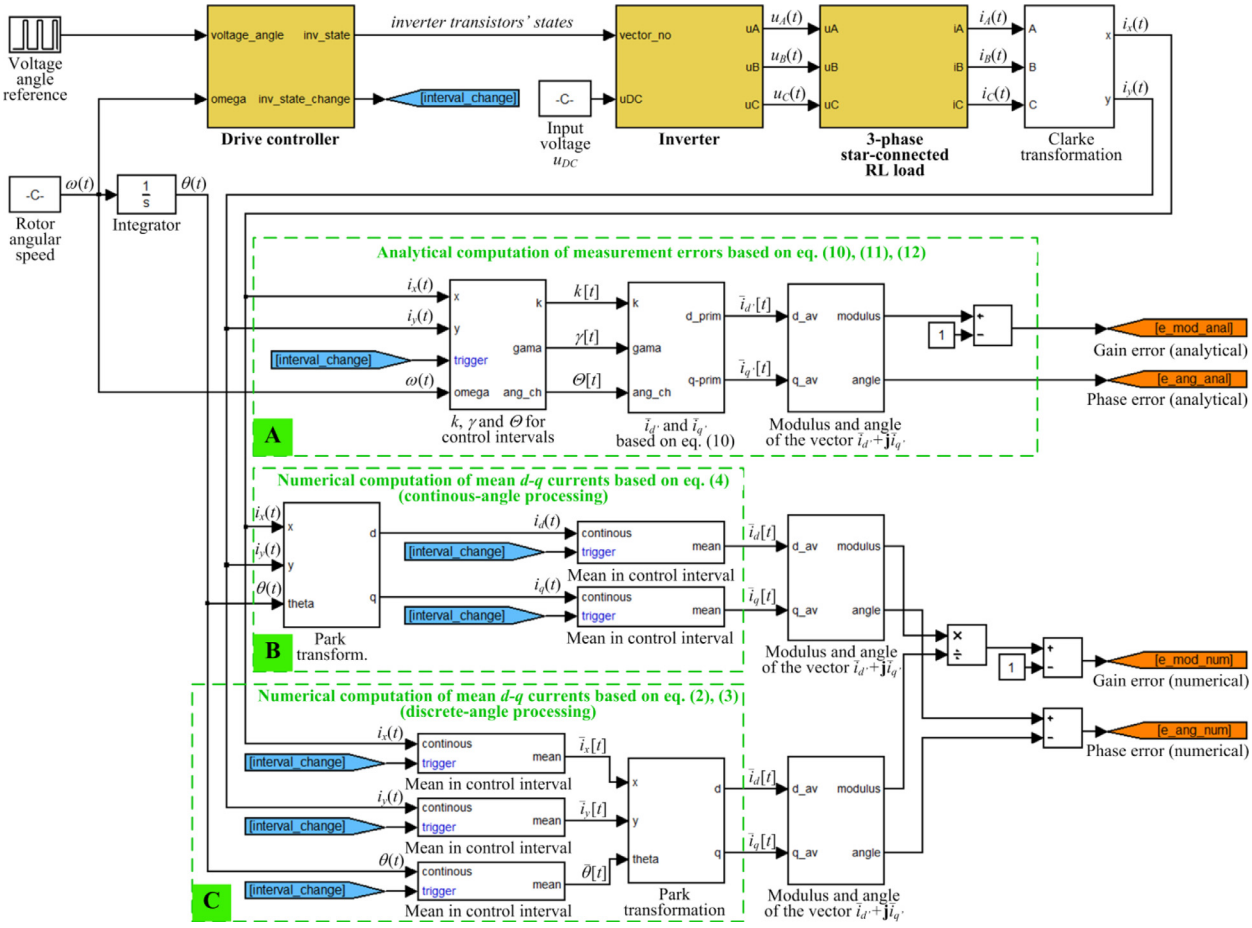

Fig. 11. Electric drive model implemented in MATLAB/Simulink.

The model is implemented in MATLAB/Simulink (Fig. 11). Constant rotor speed ω and inverter input voltage u_{DC} are assumed. Clarke and Park transforms are applied to convert the currents between *ABC*, *x*–*y*, and *d*-*q* reference frames. Exemplary waveforms of motor phase voltages and currents are shown in Fig. 12.

Continuous waveforms of motor currents $i_x(t)$, $i_y(t)$ and rotor angular position $\theta(t)$, produced by the main part of the model, are processed by three parallel processing paths (see Fig. 11). Path A computes the gain and phase errors analytically, accordingly to (10)–(12). The processing starts with deriving the variables *k*, γ, and Θ based on motor currents sampled at

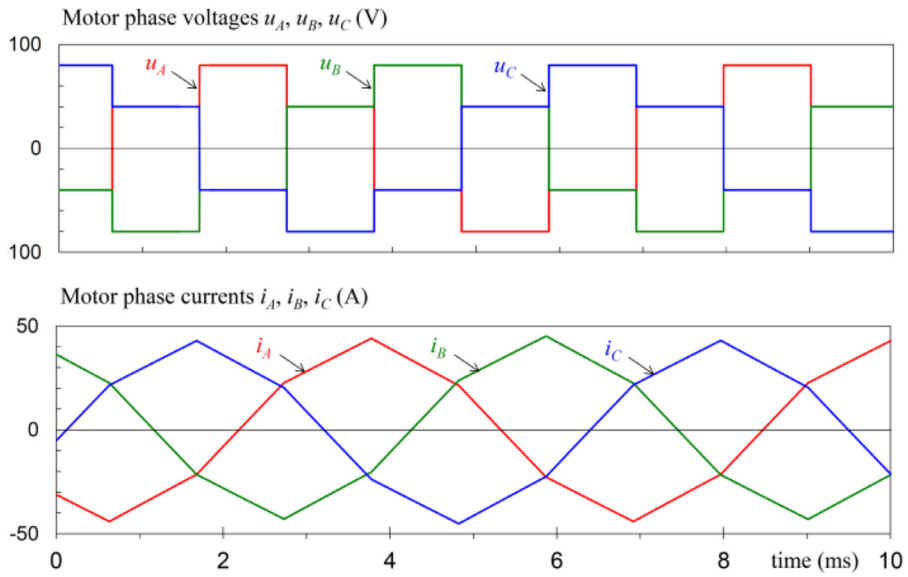

Fig. 12. Exemplary waveforms of motor phase voltages and currents during steady operation.

Table 1
Motor parameters used to validate the linear current assumption.

Parameter	Motor 1 [24]	Motor 2 [25]	Motor 3 [26]
Rated power	120 kW	22 kW	0.4 kW
Stator inductance	30.1 mH	1.9 mH	4.6 mH
Stator resistance	97 mΩ	35 mΩ	770 mΩ
Electrical time constant	310 ms	54 ms	6.0 ms

the beginning and at the end of the interval, and on the rotor speed. This makes it possible to compute MPCA-oriented current components $\bar{i}_{d'}$ and $\bar{i}_{q'}$ using (10). Finally, the gain and phase errors are derived from (11) and (12), respectively.

Processing paths B and C are used to compute the errors numerically as the reference for outcomes of path A, and they correspond to the algorithms presented previously in Fig. 3. Path B numerically computes the accurate mean current vector in *d-q* co-ordinates according to the continuous-time formula (4). It averages the continuous current components $i_d(t)$ and $i_q(t)$ to form the mean vector. Path C corresponds to the discrete-angle approach to determining the mean current vector, in which the mean stationary currents $\bar{i}_x$, $\bar{i}_y$ are transformed into *d-q* reference frame using mean rotor position $\bar{\theta}$. Paths B and C use generic motor currents $i_x(t)$, $i_y(t)$ and rotor angular position $\theta(t)$ as inputs, thus they omit all the assumptions, the normalization procedure, and the analytical solution presented in Section 4, and therefore they may be used as a reference for path A.

5.2. Validating the linear current assumption

The proposed analytical solution assumes that the phase currents change linearly during the control interval. As this assumption has recently been reported to be invalid in some cases [9], its influence on the precision of the proposed solution is investigated by grading the electrical time constant of the modeled motor. Three sets of motor parameters are selected from references (Table 1). As motor electrical time constant is related to the motor power, three motors with power ratings from a fraction of a kilowatt to over one hundred kilowatts are considered. The simulations are performed for each motor in order to evaluate how the linear current assumption influences the analytical solution when considering low, medium, and high power drives.

5.3. Simulation scenario and results

The tests focus on quantifying the differences between two current error determination algorithms: the analytical algorithm (path A) and the numerical algorithm (paths B and C). The differences are evaluated both in steady control state and during transients. The tests are repeated for three sets of motor parameters, as discussed in the previous subsection.

The simulation scenario starts with the interval of steady reference angle of voltage vector, which duration is sufficient for the current transients related to zero initial conditions to fade out. The results, shown in Figs. 13–15, cover only the last 0.1 s of this interval, and so the currents are steady. Further on, the reference angle of the voltage vector is step-changed

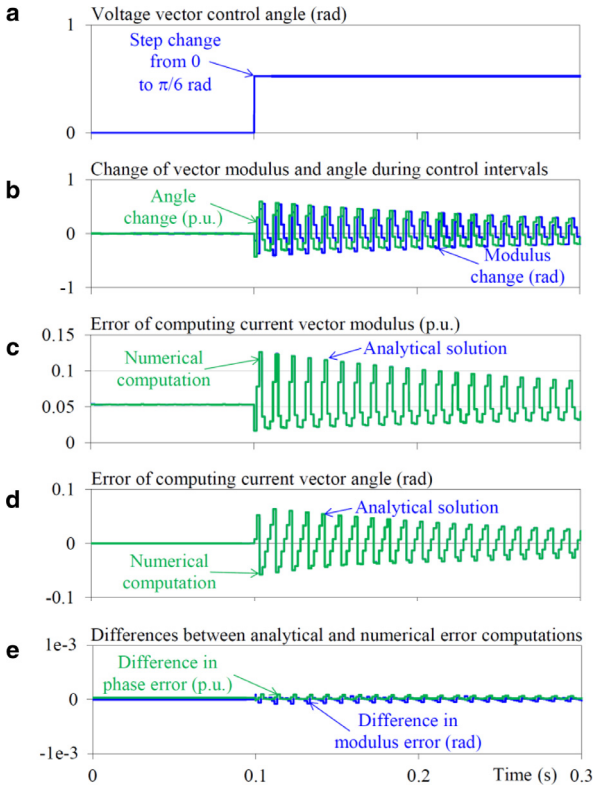

Fig. 13. Simulation results for motor 1.

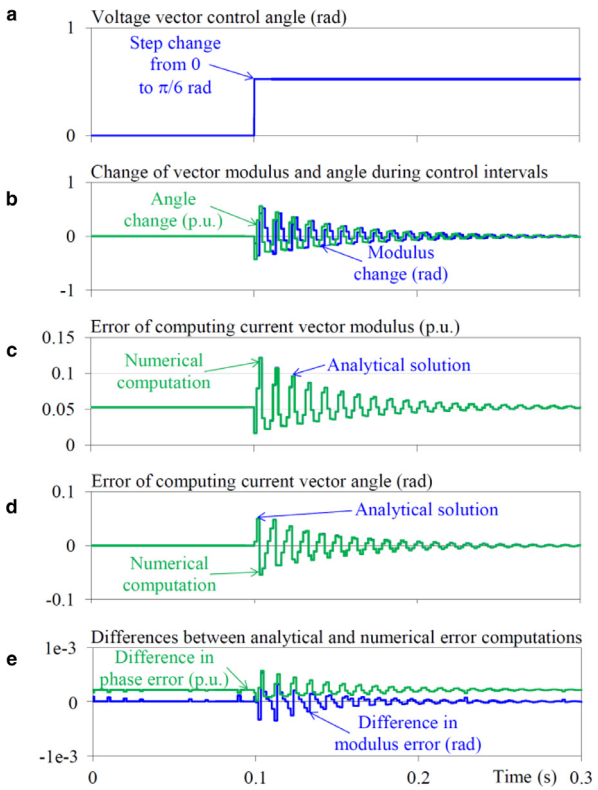

Fig. 14. Simulation results for motor 2.

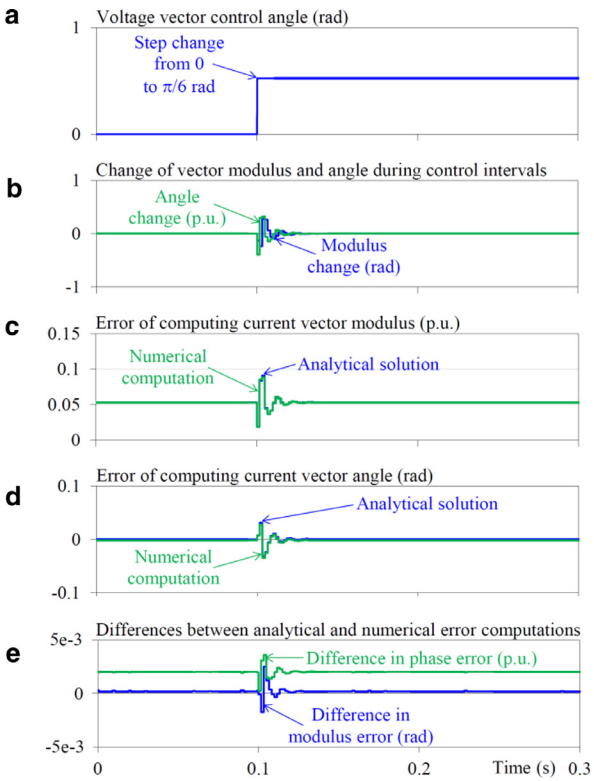

Fig. 15. Simulation results for motor 3.

Table 2
Simulation results summary.

Condition	Parameter	Motor 1	Motor 2	Motor 3
Steady state (0–0.1 s)	Difference in modulus error obtained analytically and numerically	8.6e−8 p.u.	9.5e−6 p.u.	1.9e−4 p.u.
Steady state (0–0.1 s)	Difference in phase error obtained analytically and numerically	3.5e−5 rad	2.2e−4 rad	2.0e−3 rad
Transient (0.1–0.3 s)	Peak modulus change during control interval	0.56 p.u.	0.52 p.u.	0.28 p.u.
Transient (0.1–0.3 s)	Peak angle change during control interval	0.59 rad	0.56 rad	0.39 rad
Transient (0.1–0.3 s)	Peak error of current vector modulus (obtained analytically)	1.3e−1 p.u.	1.2e−1 p.u.	9.1e−2 p.u.
Transient (0.1–0.3 s)	Peak error of current vector angle (obtained analytically)	6.4e−2 rad	5.4e−2 rad	3.1e−2 rad
Transient (0.1–0.3 s)	Maximal difference between modulus errors obtained analytically and numerically	1.0e−4 p.u.	5.3e−4 p.u.	2.5e−3 p.u.
Transient (0.1–0.3 s)	Maximal difference between phase errors obtained analytically and numerically	9.8e−5 rad	5.7e−4 rad	3.6e−3 rad

from 0 to $\pi/6$ rad, as seen in the (a) graphs. In the modeled system, such a step change induces an oscillating current response as previously reported in [15]. The step value was selected to induce oscillations featured by the peak change in current vector modulus at a level of 0.5 p.u. and the peak change in current vector angle at a level of 0.5 rad. Obviously, the peak values relate to the electrical time constant, so they differ slightly for motors 1, 2, and 3, as seen in the (b) graphs of Figs. 13–15 and in Table 2.

The results of the analytical solution well match the numerical outcomes as shown in graphs (c) and (d) of Figs. 13–15. The presented waveforms of modulus and phase errors are consistent. In the selected scale, the slight differences between analytical and numerical results can only be noticed in case of motor 3 (Fig. 15c and d). Thus, the differences are magnified in the (e) graphs and summarized in Table 2.

The numerical results confirm that at steady state the modulus has an error of 5.3%, and simultaneously that the phase error is negligible. As expected, the difference between errors obtained numerically and analytically increases with the decrease of motor power. Nevertheless, even for the 0.4-kW motor, the differences are less than 2e−4 p.u. (0.4‰) and 2 mrad, respectively for modulus and phase. Considering typical industrial electric drives, such differences are below the sensitivity of measurements.

For the modeled transient, the peak errors of discrete-angle computation are at the level of 0.1 p.u. (10%) for modulus and 50 mrad for phase, and the differences between errors obtained analytically and numerically are higher than for steady state. The peak differences for motors 1 and 2 are below 1e−3 p.u. (1‰) in modulus and 1 mrad in angle. Considering that these differences are approximately 100 times less than the determined errors, the assumption of linear current changes is

well justified here. In the case of motor 1, the assumption of the linear current changes causes higher differences between analytical and numerical outcomes. These differences are the order of few permilles and few milliradians for modulus and angle, respectively. Still the proposed solution is much more precise than the discrete-angle formula.

6. Conclusion

The paper indicates that the present approach to computing the field-oriented current vector, based on the discrete-angle formula, is not proper for high-speed drives operating in the six-step mode. The errors related to discretizing rotor angular position exceed 5%, even under steady drive operation. This must not be neglected, as improper feedback directly impacts on a drive's performance.

The main contribution of the paper is the methodology for deriving errors related to the use of discretized rotor angular position in transforming the current vector into the field-oriented reference frame. The methodology consists of an assumption of linear current changes, an original approach to co-ordinates normalization, the formulation of generalized input functions, an analytical solution of the continuous-angle formula, and a definition of gain and phase errors.

Accurate mean field-oriented currents are defined by the continuous-angle transformation formula; however, in industrial drives it is not possible for the digital controller to measure and process motor variables in a continuous or quasi-continuous manner. Thus, the present approach to determining mean motor phase currents and the discrete-angle transformation formula can be sustained if the outcomes are later refined based on the approach presented in this paper.

The assumption of linear current, which has been questioned in the recent reference, is validated by computer simulation. The validation proves that for the proposed methodology this assumption is justified when considering medium and high power drives. In low power systems, characterized by small electrical time constant, the assumption causes considerable inaccuracy, yet it still enables computing the mean currents much more precisely than the commonly applied discrete-angle approach.

As the paper aims at revising the current processing methodology, the validation by computer simulation is considered suitable. The simulation enabled quantifying the differences between accurate current and the outcomes of the proposed analytical solution, which are fractions of a permille. This would not be possible in an experiment in which the current measurement is affected by numerous disturbances.

This work focuses on current behavior during a six-step drive operation. Future work will aim at modeling motor currents upon voltage modulation, i.e. multiple changes in motor supply voltages during a control period. This is motivated by the fact that selected applications of drives do not use the six-step control, but still their rotor angle may advance during a control interval by as much as 0.7 rad [27] when they operate at high speed. The analysis of such a case must reflect current ripples related to multiple voltage changes during a control interval, which makes the formal description difficult.

References

[1] J. Vittek, P. Butko, T. Fedor, E. Struharnansky, B. Ftorek, Two cost functions evaluation for energy optimal position control with constant and linear torques, in: 2015 International Conference on Electrical Drives and Power Electronics (EDPE), 2015, pp. 13–18, doi:10.1109/EDPE.2015.7325262.

[2] A. Steimel, Power-electronics issues of modern electric railway systems, Adv. Electr. Comput. Eng 10 (2010) 3–10, doi:10.4316/aece.2010.02001.

[3] K.H. Nam, AC Motor Control and Electrical Vehicle Applications, 1 edition, CRC Press, 2010.

[4] C. Bharatiraja, S. Jeevananthan, R. Latha, S.S. Dash, A space vector pulse width modulation approach for DC link voltage balancing in diode-clamped multilevel inverter, AASRI Proc 3 (2012) 133–140, doi:10.1016/j.aasri.2012.11.023.

[5] D. Arun Dominic, T.R. Chelliah, Analysis of field-oriented controlled induction motor drives under sensor faults and an overview of sensorless schemes, ISA Trans 53 (2014) 1680–1694, doi:10.1016/j.isatra.2014.04.008.

[6] Y.-S. Kung, N.P. Thanh, M.-S. Wang, Design and simulation of a sensorless permanent magnet synchronous motor drive with microprocessor-based PI controller and dedicated hardware EKF estimator, Appl. Math. Model. (2015) 5816–5827, doi:10.1016/j.apm.2015.02.034.

[7] E. Persson, A new approach to motor drive current measurement, in: Proceedings 2001 4th IEEE International Conference on Power Electronics and Drive Systems, 2001, pp. 231–234. http://ieeexplore.ieee.org/xpls/abs_all.jsp?arnumber=975317.

[8] M. Kim, S.-K. Sul, J. Lee, Compensation of current measurement error for current-controlled PMSM drives, IEEE Trans. Ind. Appl 50 (2014) 3365–3373, doi:10.1109/TIA.2014.2301873.

[9] C.M. Wolf, M.W. Degner, F. Briz, Analysis of current sampling errors in PWM VSI drives, IEEE Trans. Ind. Appl 51 (2015) 1551–1560, doi:10.1109/TIA.2014.2357680.

[10] J. Böcker, O. Buchholz, Can oversampling improve the dynamics of PWM controls? in: 2013 IEEE International Conference on Industrial Technology (ICIT), 2013, pp. 1818–1824. http://ieeexplore.ieee.org/xpls/abs_all.jsp?arnumber=6505952.

[11] F. Wang, Z. Zhang, A. Davari, J. Rodríguez, R. Kennel, An experimental assessment of finite-state predictive torque control for electrical drives by considering different online-optimization methods, Control Eng. Pract 31 (2014) 1–8, doi:10.1016/j.conengprac.2014.06.004.

[12] P. Cortes, J. Rodriguez, C. Silva, A. Flores, Delay compensation in model predictive current control of a three-phase inverter, IEEE Trans. Ind. Electron 59 (2012) 1323–1325, doi:10.1109/TIE.2011.2157284.

[13] S. Morimoto, Y. Inoue, T.-F. Weng, M. Sanada, Position sensorless PMSM drive system including square-wave operation at high-speed, in: Conference Record of the 2007 IEEE Industry Applications Conference, 2007. 42nd IAS Annual Meeting, 2007, pp. 676–682, doi:10.1109/07IAS.2007.107.

[14] T. Schoenen, A. Krings, D. van Treek, R.W. De Doncker, Maximum DC-link voltage utilization for optimal operation of IPMSM, in: IEEE International Electric Machines and Drives Conference, 2009. IEMDC '09, 2009, pp. 1547–1550, doi:10.1109/IEMDC.2009.5075409.

[15] Y.-C. Kwon, S. Kim, S.-K. Sul, Six-step operation of PMSM with instantaneous current control, IEEE Trans. Ind. Appl 50 (2014) 2614–2625, doi:10.1109/TIA.2013.2296652.

[16] A. Dadashnialehi, A. Bab-Hadiashar, Z. Cao, A. Kapoor, Intelligent sensorless ABS for in-wheel electric vehicles, IEEE Trans. Ind. Electron 61 (2014) 1957–1969, doi:10.1109/TIE.2013.2266085.

[17] S. Racewicz, D.M. Riu, N.M. Retiere, P.J. Chrzan, Half-order modeling of saturated synchronous machine, IEEE Trans. Ind. Electron 61 (2014) 5241–5248, doi:10.1109/TIE.2014.2301741.

[18] T. Tudorache, I. Trifu, Permanent-magnet synchronous machine cogging torque reduction using a hybrid model, IEEE Trans. Magnet 48 (2012) 2627–2632, doi:10.1109/TMAG.2012.2198485.

[19] J. Vittek, V. Vavrúš, P. Briš, L. Gorel, Forced dynamics control of the elastic joint drive with single rotor position sensor, Autom. – J. Control, Meas., Electron., Comput. Commun 54 (2013) 337–347, doi:10.7305/automatika.54-3.160.
[20] L. Jarzebowicz, Error analysis of calculating average *d-q* current components using regular sampling and park transformation in FOC drives, in: 2014 International Conference and Exposition on Electrical and Power Engineering (EPE), Iasi, Romania, 2014, pp. 901–905, doi:10.1109/ICEPE.2014.697004210.1109/ICEPE.2014.6970042.
[21] L. Jarzebowicz, Indirect measurement of motor current derivatives in PMSM sensorless drives, Elektron. Elektrotech 20 (2014) 23–26, doi:10.5755/j01.eee.20.7.8019.
[22] A.-M. Wazwaz, The variational iteration method for solving linear and nonlinear ODEs and scientific models with variable coefficients, Cent. Eur. J. Eng. 4 (2014) 64–71, doi:10.2478/s13531-013-0141-6.
[23] G. Aslanova, A. Aslanov, E.T. Tarim, A new efficient method for solving nonlinear multi-point boundary value problems, Nonlinear Sci. Lett. A 5 (1) (2014) 45–65.
[24] K. Kondo, PMSM and IM rotational sensorless technologies specialized for railway vehicles traction, in: 2014 IEEE 5th International Symposium on Sensorless Control for Electrical Drives (SLED), 2014, pp. 1–7, doi:10.1109/SLED.2014.6844973.
[25] L. Sun, X. Wang, Z. Deng, Q. Ding, Research on stable regions of double-closed loop system for PMSM with low-pass filters, in: 2014 17th International Conference on Electrical Machines and Systems (ICEMS), 2014, pp. 1150–1156, doi:10.1109/ICEMS.2014.7013644.
[26] Z. Wang, J. Chen, M. Cheng, Y. Zheng, Fault tolerant control of paralleled voltage-source inverters fed PMSM drives, IEEE Trans. Ind. Electron (2015) 4749–4760, doi:10.1109/TIE.2015.2403795.
[27] S.K. Sahoo, T. Bhattacharya, Rotor flux-oriented control of induction motor with synchronized sinusoidal PWM for traction application, IEEE Trans. Power Electron 31 (2016) 4429–4439, doi:10.1109/TPEL.2015.2475398.